

Compaction Mechanism as the Function of Atomized Powder Particle Size

M. Radeka,^a J. Ranogajec,^b R. Marinković-Nedućin,^b & B. Živanović^c

^aFaculty of Technical Sciences, ^bFaculty of Technology, University at Novi Sad, Novi Sad, Serbia, ^cCenter for Multidisciplinary Study, University at Belgrade, Belgrade, Serbia

(Received 17 March 1994; accepted 25 October 1994)

Abstract: The cold compaction process of spray dried powder for ceramic floor/wall tiles production was followed by compaction response and compaction rate diagrams. Seven fractions of defined size, as well as the industrial powder batch, were compacted at pressures up to 31.5 MPa. The effect of particle size, textural and morphological characteristics on the consolidation mechanism was investigated. Both plastic deformation and brittle fracture were identified, the dominating mechanism in a given pressure range being the direct function of the size and morphology characteristics of the particles.

INTRODUCTION

Three main mechanisms in cold compaction of spray dried powder in ceramic floor and wall tile processing could be recognized: packing, plastic deformation and brittle fracture. Rearrangement and packing of the particles play an important role in all stages of the compaction process, i.e. in the whole range of applied pressures. Two other mechanisms are the function of both applied pressure and deformability of the particles. Numerous factors define the deformability of the particle: phase composition, morphology, size, water content in the particle, characteristics of binder, etc.^{1–3}

In this work the effect of the particle size on the deformability was investigated, also taking into account other characteristics of the defined size range of the same industrial powder batch (chemical and phase composition, morphology and textural characteristics). Compaction response and compaction rate diagrams were used to follow the consolidation process^{4–6} with the aim to indicate the dominating mechanism governing the compaction of particular size fractions. The dominating mechanism of consolidation in the particular pressure range was defined as the basis for optimization of particle size distribution and establishing the lowest pressure necessary for proper consolidation.

EXPERIMENTAL

Material

Ceramic atomized powder, the mixture of clay minerals, quartz, carbonates, feldspars and mica minerals, from the industrial raw material batch for ceramic tile production, was used in all the experiments. The atomized powder was separated by sieving in seven fractions of a defined size range (Table 1). Chemical and phase composition and textural properties of each fraction were determined (Tables 1 and 2).

Compaction

Compaction of defined size fractions (I–VII) and of the average sample from industrial batch (average sample) was carried out in a steel die using an Instron 1122 Press, with a crosshead speed of 50 mm/min, in the pressure interval up to 31.5 MPa. The dimensions of the obtained compacts were $d = 10$ mm and $h = 6.5$ mm.

The standard compaction response diagrams, density of compact versus applied pressure, were obtained indirectly, by screening the compaction route (crosshead displacement depending on applied force). Knowing the height of the load, its weight and dimensions of the die, the density of

Table 1. Chemical compositions of fractions I–VII and the average sample

Fraction and size range (μm)	Loss of ignition 1000°C	SiO ₂ (wt.%)	Al ₂ O ₃ (wt.%)	Fe ₂ O ₃ (wt.%)	CaO (wt.%)	MgO (wt.%)	Na ₂ O (wt.%)	K ₂ O (wt.%)	Σ (wt.%)
I <63	12.68	52.23	16.77	3.19	8.29	3.90	1.25	2.05	100.4
II 63–90	12.99	52.86	15.38	2.71	8.77	4.33	1.00	2.15	100.2
III 90–200	13.25	52.28	14.61	2.79	8.90	4.07	1.38	2.39	99.97
IV 200–315	13.06	52.64	14.25	3.35	8.97	4.43	1.11	2.20	100.0
V 315–400	12.82	54.17	14.97	3.03	6.72	5.12	1.27	2.07	100.2
VI 400–500	13.14	53.53	16.04	2.31	7.41	4.03	1.42	2.45	100.4
VII >500	13.29	53.66	15.04	3.11	7.14	3.91	1.46	2.34	99.95
Average sample	12.35	53.57	13.16	4.30	4.09	7.42	1.07	2.18	98.14

the resulting compact was computed. For better understanding of the specific mechanism of compaction, the compaction rate diagrams, $dD/dp = f(p)$, were analyzed for each of the powder fractions and the average sample.

Methods

Phase composition was determined by using X-ray powder diffraction (Philips PW 1050, CuK α). Particle size distribution was tested by standard sieving procedure. The surface area was determined by static low temperature nitrogen adsorption (ASAP 2000, Micromeritics) and microstructure by SEM (JOEL ISM 35).

RESULTS AND DISCUSSION

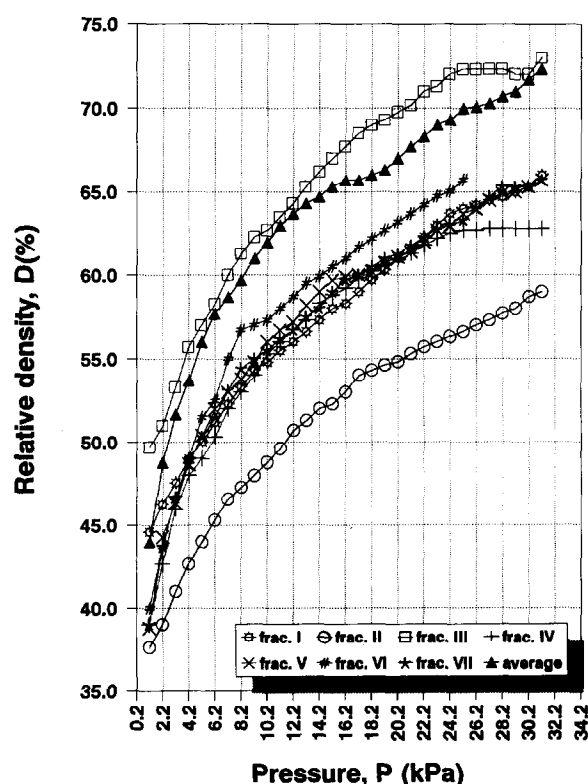
X-ray diffraction patterns of the average sample and specific fractions show the presence of quartz, calcite and dolomite, orthoclase, albite, anorthite, chloride, illite and mica minerals in all the samples, without pronounced differences in the quantitative

Table 2. Physical characteristics of fractions I–VII and the average sample

Sample	Portion in average sample (wt.%)	Density (kg/m ³)	Surface area (m ² /g)
I	1.02	2746	11.8
II	1.40	3020	13.1
III	25.80	2330	15.3
IV	25.20	2700	15.2
V	21.90	2700	14.4
VI	17.20	2700	14.8
VII	7.60	2700	14.5
Average sample	—	2700	13.7

ratio of the phases in different fractions. Chemical composition and textural properties (Tables 1 and 2) show some differences among the fractions, but are far from being the significant parameters governing the cold compaction process as shown in our previous investigation of similar systems.⁷

Compaction response diagrams for all analyzed size ranges/fractions of the powder and average sample are presented in Fig. 1. The integral curves have similar shape, but there are differences in the behavior of particular fractions concerning: (i)

**Fig. 1. Compaction response diagrams of fractions I–VII and the average sample.**

total relative density increase in the applied pressure interval and (ii) position of inflection points of the curves.

Concerning total density increase, the behavior of fractions I, IV, V and VII is practically identical, fraction VI having just slightly higher values.

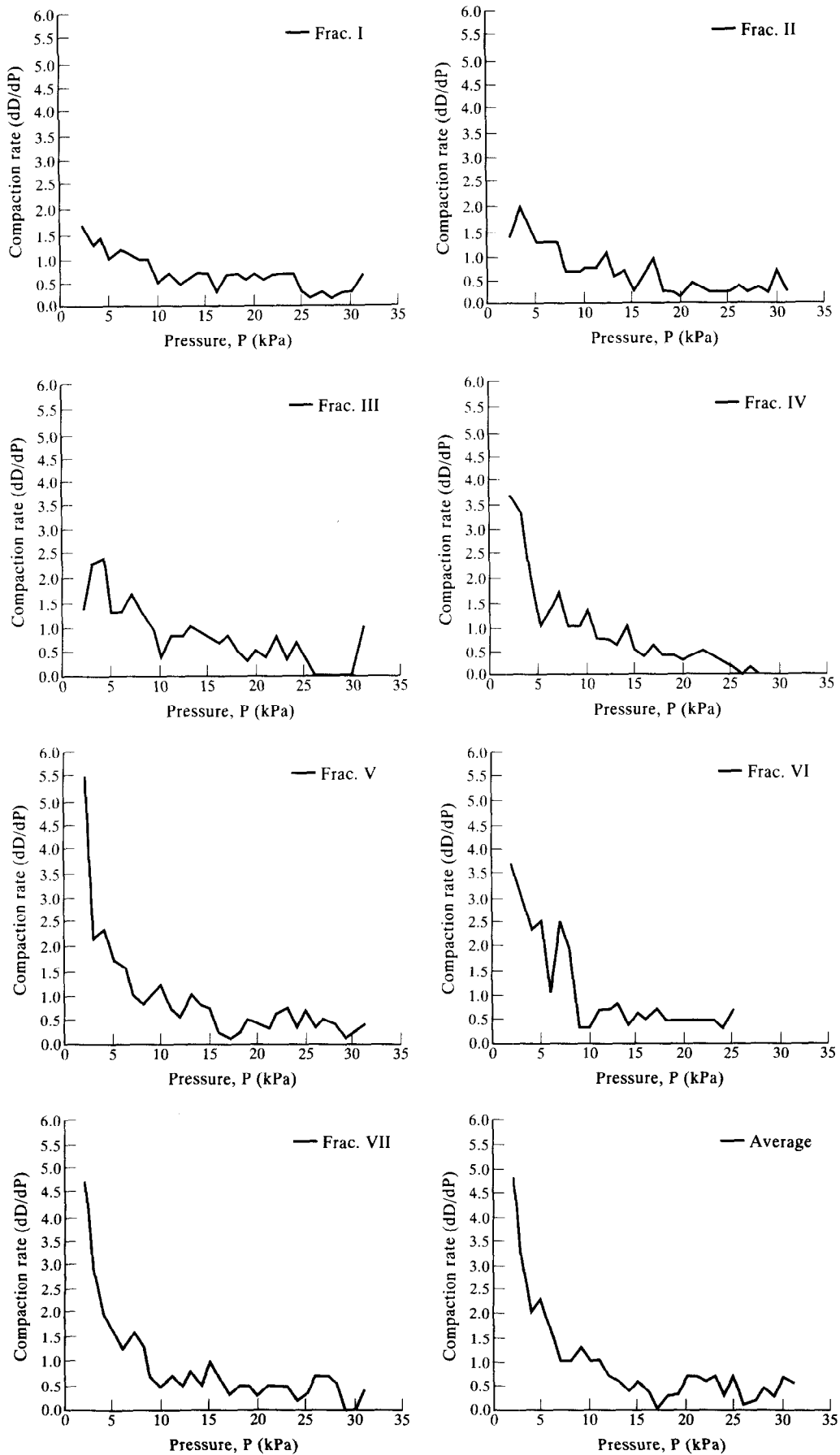


Fig. 2. Compaction rate diagrams of fractions I-VII and the average sample.

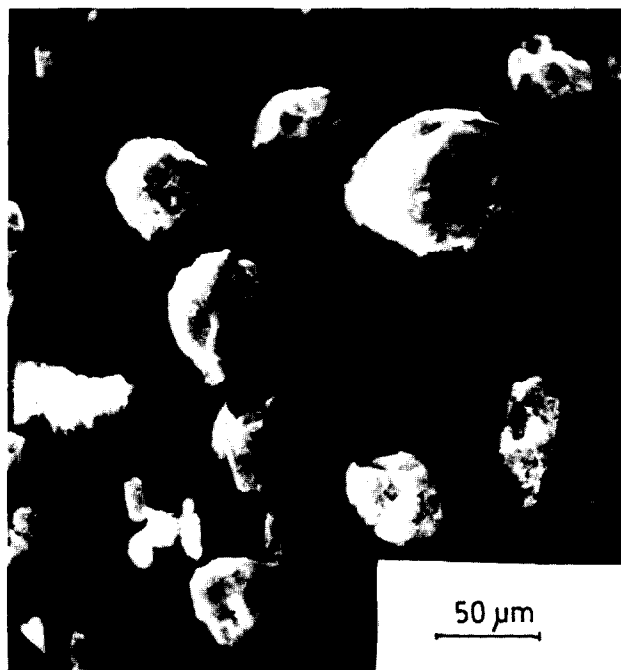


Fig. 3. SEM micrograph of the initial powder of fraction I.

Fraction II has the lowest and fraction III the highest density in the whole interval of applied pressures; the average sample has density values between fraction III and the group of fractions of similar behavior. This kind of different behavior could not be explained on the basis of particular size differences of the fractions only. So, the size, geometry and morphology of the fractions have to be considered together as critical parameters of particles concerning the mechanism of compaction in a particular pressure region.⁸

The compaction rate diagram, the first deriva-

tive of integral density increase curve, is considered as a useful tool for better understanding of the processes taking place during compaction.⁶ Namely, the inflection points on integral curves could be considered as an indication of the change of the mechanism governing the compaction process in a defined pressure interval. The maxima on the differential curve position precisely these points. The locations of the maxima, the shapes of the peaks, as well as the magnitude of the rate of density increase, contain important information about the compaction process. The differential curves of the powder fractions are presented in Fig. 2.

The compaction rate curve of fraction I is characterized by a relatively low initial densification rate, with no pronounced differences concerning the rate in the whole pressure interval (Fig. 2/I). SEM micrograph of the initial powder (Fig. 3) shows that this fraction is a mixture of irregularly shaped and spherical particles. One could expect dense packing of these low-size particles, the density being somewhat lower than expected because of the dominant highly irregularly shaped particles in combination with full spheres. According to the presented results it could be supposed that the dominant mechanism of the compaction process is packing and plastic deformation, as shown also by SEM investigations of the samples after pressing at 6.4 and 10.2 MPa (Fig. 4). The behavior of fraction II is quite similar, as judged from the compaction rate diagram (Fig. 2/II). Lower total density, as previously stated, is a consequence of the increased size of the particles.

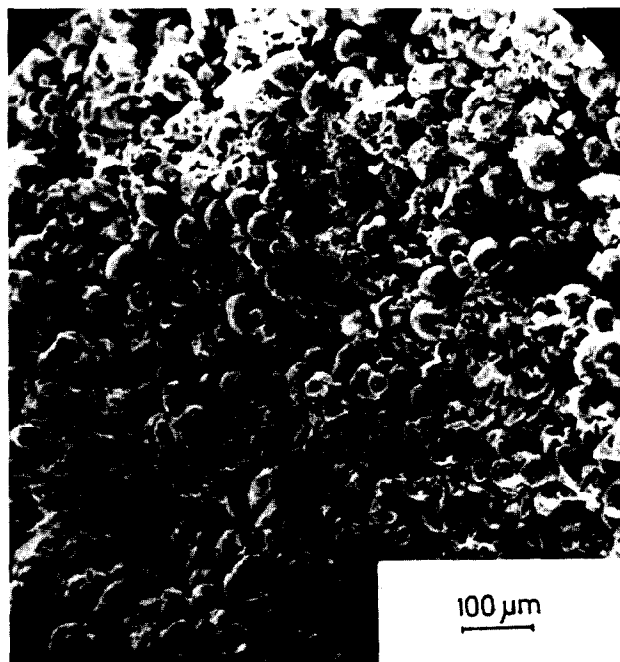
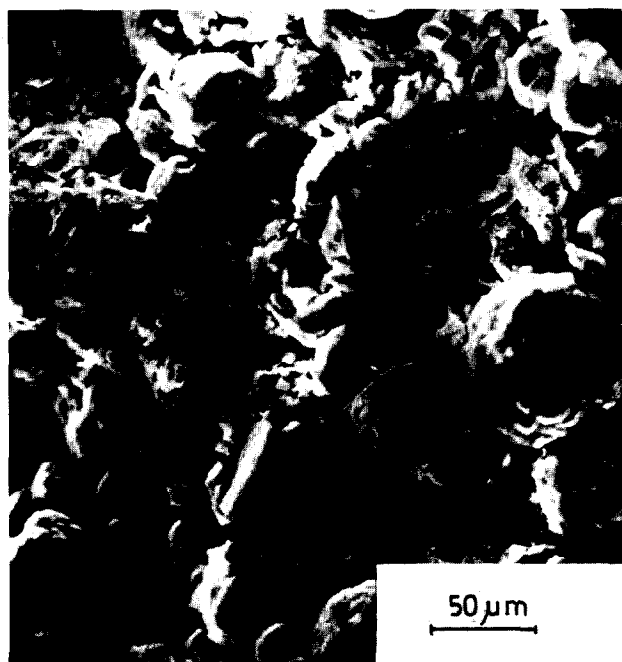


Fig. 4. SEM micrographs of fraction I, pressed at: (a) 6.4 MPa; (b) 10.2 MPa.

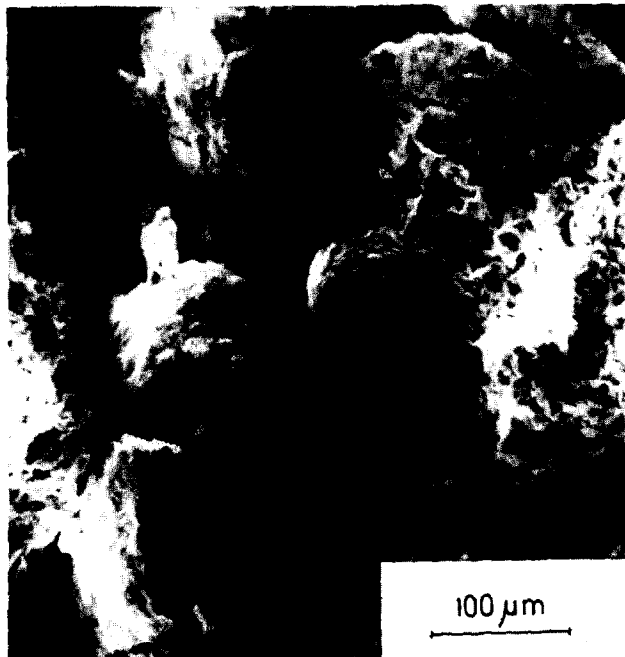
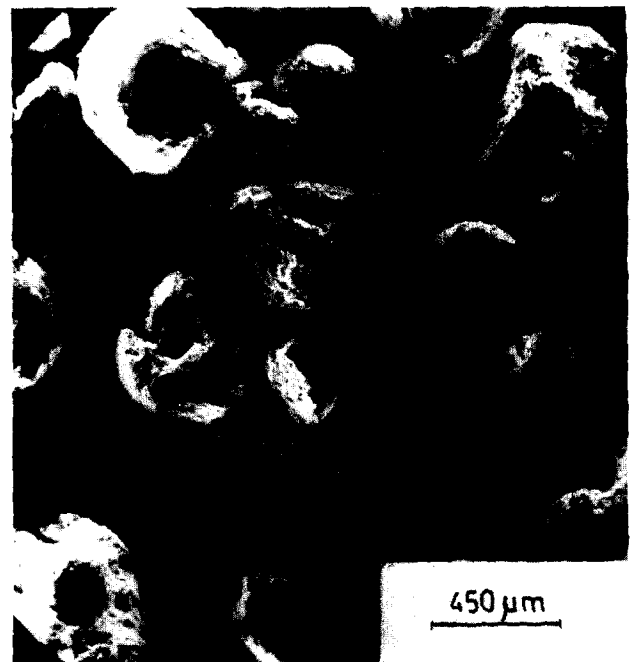


Fig. 5. SEM micrograph of fraction IV, pressed at 10.2 MPa.

In the case of fraction III, there are two inflections in the low pressure range, shown by two relatively sharp maxima on the differential curve (Fig. 2/III), indicating that brittle fracture starts to play an important role in the compaction process. The lowest value of the density of this fraction (Table 2) speaks in favor of considerable porosity of the particles comprising this fraction. The presence of a sharp maximum at high pressure (Fig. 2/III) is a consequence of the fragmentation of previously deformed particles. Fraction IV is characterized by a higher initial rate of density increase

(Fig. 2/IV). There is a fracture and consecutive crush of the particles already at lower pressures (three relatively sharp maxima on the rate curve). It is also shown by SEM micrographs of the sample compacted at 10.2 MPa, that there are some intergranular pores remaining (Fig. 5). The mixture of plastic deformation and brittle fracture is combined in the case of this fraction of intermediate particle size. Similar behavior is observed in fraction V (Fig. 2/V).

Further increase of the particle size brings about a change in the dominant compaction



(a)



(b)



Fig. 6. SEM micrograph of the initial powder of fraction VII.

Fig. 7. SEM micrograph of fraction VII, pressed at: (a) 3.8 MPa; (b) 10.2 MPa.

Table 3. Relative density increase in different pressure intervals

Sample	$\Delta D/\Delta D_{\max}$ (%) (0–1.3 MPa)	$\Delta D/\Delta D_{\max}$ (%) (1.3–7.6 MPa)	$\Delta D/\Delta D_{\max}$ (%) (7.6–23.0 MPa)
I	29.5	32.3	38.2
II	2.2	50.5	47.3
III	17.8	42.2	39.9
IV	8.0	54.4	37.6
V	10.6	54.0	35.4
VI	9.8	56.9	33.3
VII	14.4	53.9	31.7
Average sample	21.8	46.7	31.5

mechanism, depicted by both the integral and differential density curve. The sharp maxima at lower pressures indicate brittle fracture as the mechanism prevailing in sample densification. This is even more obvious in fraction VII, characterized by the presence of clusters and hollow particles in the initial powder (Fig. 6). The differential curve and SEM micrographs show that crushing of the hollow particles occurs already at lower pressures (Fig. 2/VII and Fig. 7(a)), brittle fracture being the dominant mechanism of the compaction process. The larger agglomerates, however, remained unaffected with regard to fracturing, but there is the intrusion of smaller particles, originating from the fragmentation process, into the pores of the cluster particles (Fig. 7(b)).

The increase of the density up to the pressure of 7.6 MPa ($\Delta D/\Delta D_{\max}$) shows that even at this relatively low pressure interval (ca. 25% of the maximal pressure) the main densification occurs (Table 3). The different mechanisms of densification among different fractions, as stated previously, bring about the gradual increase of density with increasing particle size in this pressure interval. Further support of differing mechanisms is obtained by analyzing the size distribution among each of the green compacts after pressing at 6.4

Table 4. Size composition of the green compacts obtained at 6.4 MPa

Sample	Particles larger than initial fraction (wt.%)	Particles smaller than initial fraction (wt.%)
I	25	—
II	11	—
III	—	4
IV	2	8
V	18	30
VI	—	43
VII	—	30

Table 5. Surface of the initial powder and the corresponding green compact obtained at 6.4 MPa

Sample	Surface area of initial powder (m ² /g)	Surface area of green compacts (m ² /g)	Increase of surface area (%)
II	15.2	15.96	5
VI	16.0	18.98	18.5

MPa. For that purpose the green compacts, being loosely bound, were broken apart by slight finger-pressing; after treatment in a sieve shaker for 20 min, size composition of these systems was determined (Table 4). The interpretation of the results is based on the supposition that plastic deformation and packing will result in particle agglomeration over the original size range, while brittle fracture will bring about an increase in the content of smaller particles. The results show that the dominant mechanism for fractions I and II is a mixture of packing and plastic deformation, the fragmentation mechanism dominating in fractions VI and VII. The middle fractions, thanks to the presence of both mechanisms (plastic deformation and brittle fracture) show both agglomeration and fragmentation of the original particles. The surface area data of the initial powder and corresponding green compacts obtained at 6.4 MPa (Table 5) show the difference in the area increase for particular fractions (II and VI), confirming the importance of the crushing process in the larger fractions even in the low pressure region. The increased surface area also contributes to the number of contacts among particles, not only as the initial step in densification during pressing, but also being important in the following sintering process.

CONCLUSIONS

Both plastic deformation and brittle fracture, combined with packing of the particles, have been determined as densification mechanisms in ceramic atomized powder during cold compaction. In the fractions with the smallest particles the dominating mechanism of consolidation is a mixture of packing and plastic deformation. The transition from plastic deformation to brittle fracture occurs in the particle size range between 90 and 200 μm . For fractions with particle sizes between 90 and 400 μm a mixture of both mechanisms, i.e. plastic deformation and fracture, is confirmed, while in the largest fraction fragmentation and crushing characterize the cold compaction process.

REFERENCES

1. COUPELLE, P., DESTERMES, J. & BAUMARD, J. F., Deformation of spray-dried agglomerates and compaction behavior of spray-dried powders. *Ceram. Acta*, **5** (1993) 23–28.
2. ZHAO, J. & HARMER, M. P., Effect of pore distribution on microstructure development: I. Matrix pore. *J. Amer. Ceram. Soc.*, **71** (1988) 113–20.
3. ZHAO, J. & HARMER, M. P., Effect of pore distribution on microstructure development: II. First and second-generation pores. *J. Amer. Ceram. Soc.*, **71** (1988) 530–9.
4. MESSING, G. L., MARKHOFF, C. J. & McCOY, L. G., Characterization of ceramic powder compaction. *Ceram. Bull.*, **61** (1982) 857–60.
5. MATSUMOTO, R. L. K., Generation of powder compaction response diagrams. *J. Amer. Ceram. Soc.*, **69** (1986) C-246–7.
6. MATSUMOTO, R. L. K., Analysis of powder compaction using the compaction rate diagram. *J. Amer. Ceram. Soc.*, **73** (1990) 465–8.
7. RANOGAJEC, J., MARINKOVIĆ-NEDUČIN, R., KASAŠ, K. & ŽIVANOVIĆ, B., Correlation between atomized powder composition and final floor tile density. *Amer. Ceram. Soc. Bull.*, **71**(2) (1992) 208–12.
8. RANOGAJEC, J., MARINKOVIĆ-NEDUČIN, R., PANIĆ, J., KASAŠ, K. & ŽIVANOVIĆ, B., Compaction rate diagrams of multicomponent ceramic powder. *Ceram. Engng Sci. Proc.* (in press).